Materials Advances

ROYAL SOCIETY OF CHEMISTRY

PAPER

View Article Online
View Journal | View Issue

Cite this: *Mater. Adv.*, 2023, 4, 2971

Synthesis and rheological investigations of gum-ghatti-cl-poly(NIPA-*co*-AA)-graphene oxide based hydrogels†

Pragnesh N. Dave, *[a] Pradip M. Macwan[b] and Bhagvan Kamaliya[a]

The purpose of the present work is to study the rheological properties of gum ghatti-cl-poly(NIPA-*co*-AA)/GO (GNAGO) hydrogels reinforced with graphene oxide (GO) to modify their mechanical and thermal properties. The GNAGO hydrogel was characterized by SEM and the thermal stability of the hydrogel was examined by TGA measurements. The study of the storage (G') and loss (G'') modulus shows that the gum ghatti-cl-poly(NIPA-*co*-AA)/GO (GNAGO) acts elastically in nature. The results showed that gum ghatti-cl-poly(NIPA-*co*-AA)/GO hydrogels showed greater viscoelastic properties than the gum ghatti-cl-poly(NIPA-*co*-AA) hydrogel. A decrease in viscosity with the increase in shear rate confirms the non-Newtonian behavior of the hydrogels. The determined covalence crosslinking is confirming the solid-like behavior and elastic nature ($G' > G''$). The flow properties of the hydrogel were studied using rheological models (Herschel–Bulkley and Power law) and based on the R^2 value, both of the models were found to be best fitted. Furthermore, the damping factor ($\tan\delta$) was found to be close to 0.35, indicating that the damping of the materials has been improved due to the interlocking and penetration of GO particles within the hydrogel. The results of this work provided great insight into understanding the relationship between microstructure and mechanical performance of hydrogels and these materials can be applied for adsorption, and controlled drug loading and release due to the presence of GO as a drug-binding effector in the GNAGO hydrogels.

Received 28th February 2023,
Accepted 5th June 2023

DOI: 10.1039/d3ma00092c

rsc.li/materials-advances

Introduction

Graphene has piqued the interest of scientists since its discovery in 2004, due to its fascinating characteristics.[1,2] Graphene oxide (GO), a graphene derivative, has a huge surface area, a high aspect ratio, and remarkable mechanical capabilities, even though its mono-layer two-dimensional sheets include a lot of oxygen-containing groups.[1,3] Along with its hydrophilic oxygen-containing groups,[4] GO may be easily exfoliated and stably disseminated as single-layer sheets in an aqueous solution, which is advantageous for generating mechanically robust nanocomposite hydrogels. These oxygen-containing functional groups allowed GO to engage with hydrophilic polymeric composites physically and chemically, significantly improving mechanical characteristics.[3] Along with its unique features, graphene has emerged as one of the most promising nanomaterials. GO, in contrast, may be easily functionalized *via* both covalent and noncovalent bonding, making it a key building block in the synthesis of novel materials,[5] and it has also proven to be a stronger material for drug delivery systems.[4]

The *Anogeissus Latifolia* tree, a member of the *Combretaceae* family, produces the Indian gum commonly known as gum ghatti (GG) as an exudate which is widespread throughout Sri Lanka and India and is renowned for having one of India's largest forest covers. Unlike gum Arabic, GG is spontaneously extruded as larger vermiform masses or circular rips with a diameter of less than 1 cm (without tapping). As an anionic natural polysaccharide, gum ghatti has recently attracted the attention of several researchers. Alternating 4-O- and 2-O-substituted D-mannopyranose units and chains of 1 → 6 connected D-galactopyranose with side chains of L-arabinofuranose residues make up the primary structure of GG.[6] Gum ghatti is commonly used in the paper, pharmaceutical, and food industries due to its thickening and emulsifying properties. It functions as a sustained release, matrix-forming, film-forming, and mucoadhesive polymer in pharmaceutical formulations. The structural features of gum ghatti are displayed in Scheme 1.[7]

In terms of viscoelasticity, flow, consistency, adhesiveness, responsiveness to externally applied shear stress, the extent of

[a] *Department of Chemistry, Sardar Patel University, Vallabh Vidyangar-388 120, Gujarat, India. E-mail: pragnesh7@yahoo.com*
[b] *B. N. Patel Institute of Paramedical & Science (Science Division), Sardar Patel Education Trust, Bhalej Road, Anand – 388001, Gujarat, India*

† Electronic supplementary information (ESI) available. See DOI: https://doi.org/10.1039/d3ma00092c

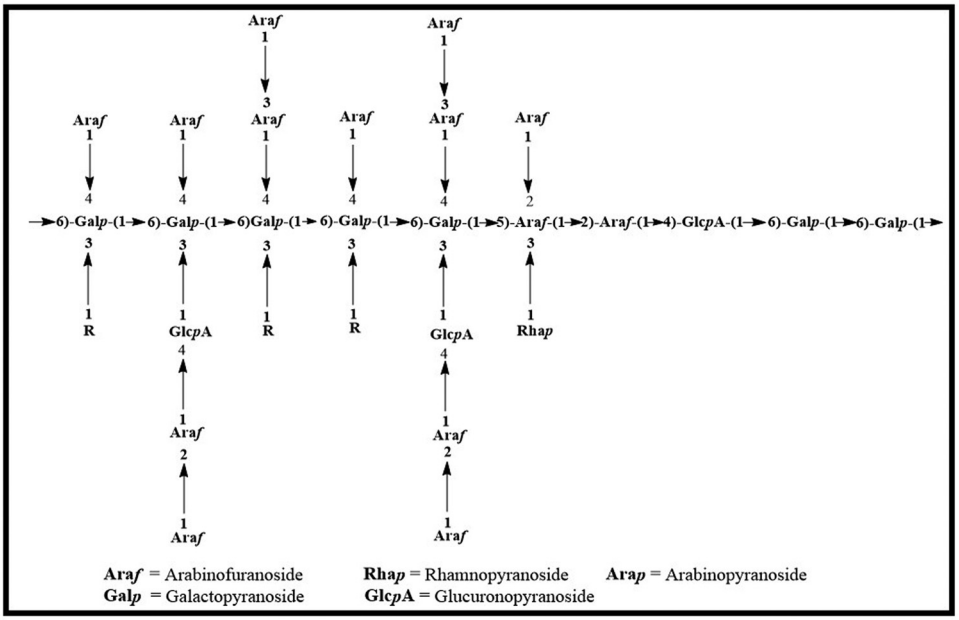

Scheme 1 Structural aspects of gum ghatti.[8]

deformation, stretchability, and recoverability, rheological characterization is the best instrument for assessing the microstructure and mechanical behaviour of hydrogels. By examining the relationship between rheological parameters based on frequency, time, content, and temperature and the microstructural arrangement of the synthesised hydrogels, rheology can provide a clear picture of how these materials can be used for various applications. Rheological approaches can be used more effectively to investigate the strength, gelation, and viscoelastic properties of hydrogels.[9,10]

Several types of polymers have been used in the preparation of hydrogels to attain reduced manufacturing costs and higher properties.[11] However, the weak mechanical properties of the hydrogels limit their applications widely. To enhance the properties of hydrogels, nanoparticles such as montmorillonite,[11] graphene oxide,[12] gold,[13] iron oxide,[14] *etc*., have been used by many researchers. Nanocomposite hydrogels include the combination of inorganic nanoparticles inside three dimensional polymeric networks. The properties of the nanocomposites can be easily adjusted by manipulating the properties of the hydrogel and the composite material.[15] Fang *et al.* used atom transfer radical polymerization to covalently connect graphene to polystyrene, resulting in improved thermal and mechanical characteristics.[16] Castelain *et al*.[17] revealed alternative chemical approaches to functionalize graphene with short-chain polyethylene, which altered the mechanical characteristics of graphene-based HDPE nanocomposites. Vasileiou *et al.*[18] used a non-covalent compatibilization strategy to describe the dispersion and characteristics of polyethylene graphene composites made from maleated linear low-density polyethylene (LLDPE) derivatives and thermally reduced GO. Luqman Ali *et al.*[19] investigations on the flow curve (shear rate, viscosity, shear stress) and flow sweep study of the GO@p(AMPS) hydrogel indicate that the material has pseudo-plastic thixotropic behavior. The outcomes from the study of storage modulus (G') and loss modulus (G'') showed that the GO@p(AMPS) behaves elastically, is a semi-solid, and is pseudo-plastic in nature. Yu *et al.*[20] created flame-retardant functionalized GO (FRs-FGO) by incorporating amine functionalized GO and a phosphoramide oligomer into PP and concurrently compatibilizing with PP-grafted maleic anhydride (PP-*g*-MA). Seo *et al.*[21] also reported the compatibility of functionalized graphene with polyethylene and its copolymers as a function of molecular weight and polarity in intriguing research.[22]

For the objective of making 2D macroassemblies, it has a range of potential applications including drug delivery,[23] tissue scaffolds,[24] bionic nanocomposites,[25] and supercapacitors.[26] Numerous groups have lately researched graphene-based hydrogels and/or composites. For instance, GO/DNA composite gels, GO/hemoglobin composite gels,[27] and GO/poly(vinyl alcohol) composite hydrogels have recently been created by the Shi group.[28] The creation of materials with incremental gains in terms of physical, chemical, mechanical, and/or material characteristics as compared to the matching native gel matrix is a particularly stringent criterion for graphene/GO composite gels.

Here we report free radical polymerization preparation of a biopolymer-based hydrogel using gum ghatti (GG), acrylic acid (AA), and *N*-isopropylacrylamide (NIPA) as monomers, as well as ammonium peroxodisulfate (APS) as an initiator, *N*,*N*,*N*′,*N*′-tetramethylethylenediamine (TEMED) as an accelerator, and *N*,*N*′-methylene bis-acrylamide (MBA). The significance of adding GO to the synthesized hydrogels was to further improve the rheological properties. This study aims to explore the potential of hydrogels made from GO gum ghatti-cl-poly(NIPA-*co*-AA). This is, as far as we are aware, the first attempt to create GO using hydrogels based on GG, NIPA, and AA. On the rheological characteristics of GG hydrogels, the effects of gum ghatti-cl-poly(NIPA-*co*-AA) substitution and mixing with GO at various

concentrations were examined. The TGA, morphological, and FTIR spectroscopic properties of these gum ghatti-cl-poly(NIPA-*co*-AA)/GO hydrogels were investigated. Significantly more drug deliveries and biological applications might be made possible using the upgraded hydrogel composition.

2. Experimental

2.1. Chemicals and reagents

Gum ghatti, acrylic acid (AA), ammonium persulfate (APS), *N*,*N*,*N*′,*N*′-tetramethylethylenediamine (TEMED) and *N*,*N*′-methylene-bisacrylamide (MBA) were purchased from Loba Chemie (Mumbai, India). Gum ghatti has a globular structure with rhamnose, arabinose, galactose and glucose in a molar ratio of 2.3 : 72.9 : 16.4 : 8.6 with 4.6% protein and 2% uronic acid. *N*-Isopropylacrylamide (NIPA) was purchased from TCI. GO was purchased from Sigma Aldrich (Munich, Germany). All the materials used in the present study were of reagent grade. In the experiments, triple distilled water was used.

2.2. Preparation of gum ghatti-cl-poly(*N*-isopropylacrylamide-*co*-acrylic acid)/GO

Hydrogels composed of gum ghatti-cl-poly(NIPA-*co*-AA) and gum ghatti-cl-poly(NIPA-*co*-AA)/GO were synthesized using free radical polymerization. GG (100 mg) first was dissolved in 10 mL of deionized water in a 100 mL beaker. Then 0–5 mg of GO was dispersed into this mixture and then the solution was sonicated for 40 min at room temperature by using ultrasonication and this mixture was then agitated by a magnetic stirrer (250 rpm). 10 mg of *N*,*N*′-methylene bis-acrylamide (MBA) as a cross-linker was added to the beaker followed by 40 mg of NIPA, 0.2 mL of AA, and 10 mL of deionized water. The beaker was then heated to 50 °C for 30 minutes. Free radicals were produced using ammonium persulfate (APS) (10 mg) as an initiator and 0.02 ml of *N*,*N*,*N*′,*N*′-tetramethylethylenediamine (TEMED) as an accelerator was added. The preliminary signal of gel formation appeared after 45 minutes. The reaction was then continued for three hours in a hot air oven for the completion of the polymerization process.[28–30] The non-reactive ingredients were removed from the hydrogels by repeatedly washing them with deionized water. The hydrogel was allowed to gradually dry for 48 hours at 50 °C and was then pulverized into powder form and then passed through a sieve with a mesh size of 250–500 μm. The above-mentioned method was used to create gum ghatti-cl-poly(NIPA-*co*-AA) hydrogels without the need for GO.[31] The possible mechanism for the synthesised hydrogel is depicted in Scheme 2.

2.3. Characterization

Thermogravimetric analysis (TGA) of the dried samples was performed using a TGA 5000/2960 TA instruments, USA, in a nitrogen environment with a heating rate of 10 °C min^{-1} and a temperature range of 30–700 °C. The morphology of the dried GO, gum ghatti-cl-poly(NIPA-*co*-AA), and gum ghatti-cl-poly(NIPA-*co*-AA)/GO hydrogels was examined using high resolution scanning electron microscope (FESEM) (Philips, Netherlands) equipment. Fourier transform infrared (FT-IR) spectroscopy of the materials was recorded on a PerkinElmer Model using the KBr plate method in the range of 400–4000 cm^{-1}. FTIR results and discussion are available in the ESI† (Fig. S2). The flow, mechanical, and viscoelastic properties, as well as the temperature dependence, were all examined using rheological experiments. The MCR 102 Rheometer (Anton Paar, Germany) with a plate-plate and cone plate system (25 mm, gap = 1 mm) was used to conduct the rheological study. A built-in Peltier device altered the sample temperature (with a precision of 0.01 °C) during the measurements. Using a

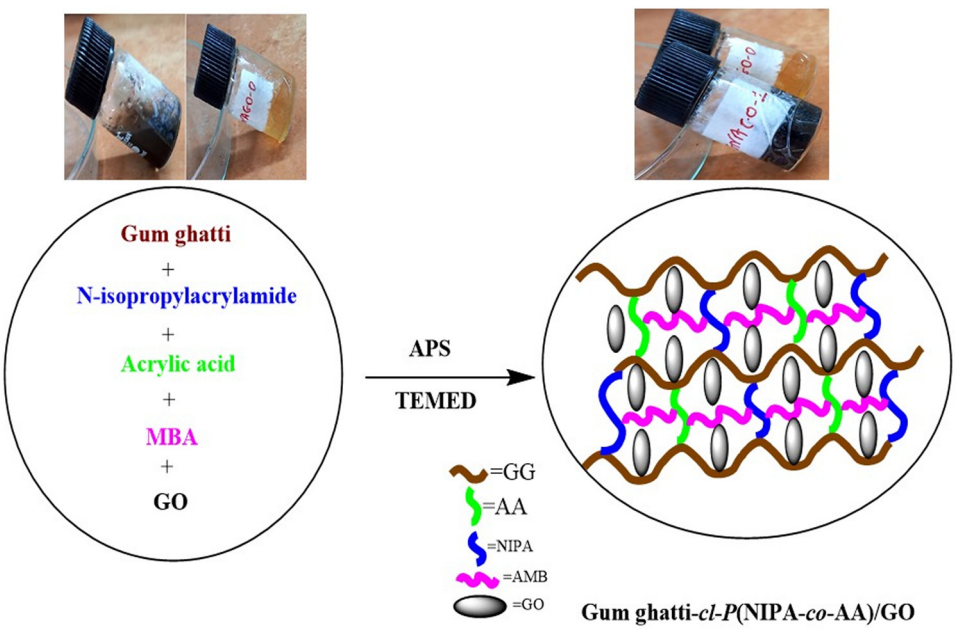

Scheme 2 Possible mechanism of gum ghatti-cl-poly(NIPA-*co*-AA)/GO hydrogels.

plate-plate rheometer, hydrogels were studied. The edges of the specimen are brought out at the measuring part to ensure that it is securely in place in the measurement position when it comes into contact with the upper plate. For the rheological measurement, all samples were utilised that had just been processed. Using a Peltier device, the experiment's temperature was controlled. The Rheoplus programme provided the data obtained from the rheometer system.

2.4. Statistical analysis

All the measured values are expressed as the mean ± SD. Statistical analysis was performed using ANOVA tests (OriginPro 2021). The level of significance was set at $p < 0.05$.

3. Results and discussion

3.1. Scanning electron microscope (SEM)

Fig. 1 displays SEM images of hydrogels prepared from gum ghatti-cl-poly(NIPA-*co*-AA), GO (GO), and gum ghatti-cl-poly-(NIPA-*co*-AA)/GO. Due to scratch and disassembly, the GO has a multi-layered, disordered structure, as shown in Fig. 1(a), as well as a pleated sheet-like structure;[32] in addition it has a wrinkled sheet-like structure due to exfoliation.[32] This could play a favorable role in improving the interlocking of the peels with each other and allow strong interaction with the subsequent GG. The solid GO sample is severely agglomerated because of its high specific surface area and the strong interlocking of the peels.[33]

The SEM images of the gum ghatti-cl-poly(NIPA-*co*-AA) hydrogel (Fig. 1b) demonstrate smooth (orange arrow) and rough (red arrow) regular surface shapes before the addition of GO into the hydrogel. In the case of the gum ghatti-cl-poly(NIPA-*co*-AA)/GO hydrogels, they are rough and folded with more defined porous structures (Fig. 1c). The surface morphology of gum ghatti-cl-poly(NIPA-*co*-AA)/GO hydrogel demonstrated significant changes, and the porous 3-D network structure of the hydrogels spread in an irregular manner on the rough surface was observed. Surface with significant spaces (orange arrow) was predicted in gum ghatti-cl-poly(NIPA-*co*-AA)/GO in comparison with GG, which increases the penetrability of pollutants as well as their easier movement throughout the cross-linked network of the hydrogel. This resulted in an increase in the adsorption amount and usage of the hydrogel. Enhanced crosslinking interactions and stabilized network structures are due to the presence of GO in the hydrogel.[33] This feature would allow quicker absorption of substances such as drugs and dyes, reflecting one of the advantageous properties of these materials as adsorbents.[34] Additional SEM images for the GNAGO-0 and GNAGO-3 hydrogel samples are provided as the ESI† (Fig. S3).

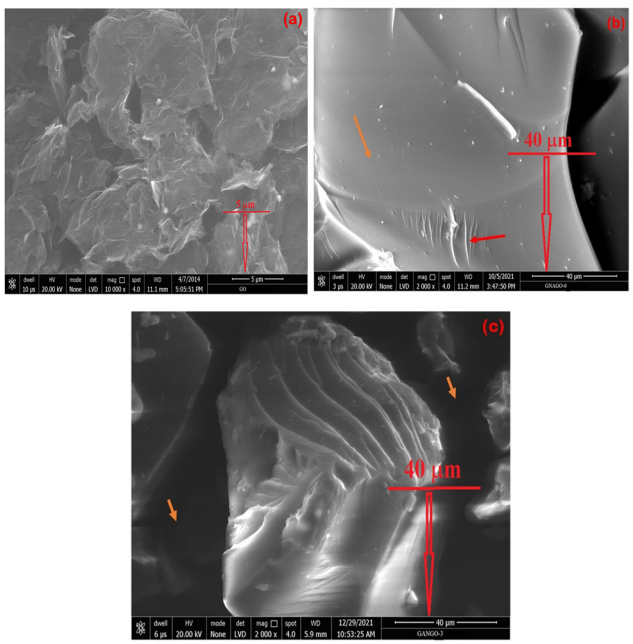

Fig. 1 Scanning electron microscope images of (a) GO, (b) gum ghatti-cl-poly(NIPA-*co*-AA) hydrogel and (c) the gum ghatti-cl-poly(NIPA-*co*-AA)/GO hydrogel composite.

3.2. Thermogravimetric analysis (TGA)

The thermogravimetric method was used to investigate the influence of GG, GNAGO-0 and GNAGO-3 hydrogel samples, as shown in Fig. 2. The hydrogels containing GO demonstrate greater thermal stability than the hydrogels without GO, and this thermal stability reflects the better interaction between GO groups and macromolecular acrylic acid (AA) chains. The TGA curves clearly show that the GNAGO-3 has more thermal stability than both the pure GG and the GNAGO-0. The TGA of GG revealed a two-stage breakdown. The initial decomposition temperature (IDT) of GG was 227 °C, while the final decomposition temperature (FDT) was 443 °C.[35] GNAGO-0, on the other hand, demonstrated IDT at 190 °C and FDT at 480 °C. The IDT of pure GG was found to be greater, but the FDT was lower than that of GNAGO-0. GNAGO-3, on the other hand, demonstrated IDT at 200 °C and FDT at 510 °C. The copolymerization TGA spectrum shows three stages of degradation. The first stage was caused by moisture or water content loss, and it ended at 200 °C.[36] The second stage that

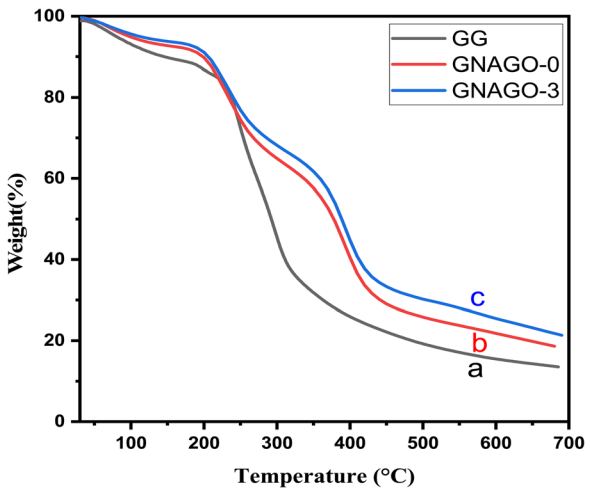

Fig. 2 TGA curves for (a) GG, (b) the gum ghatti-cl-poly(NIPA-*co*-AA) hydrogel and (c) the gum ghatti-cl-poly(NIPA-*co*-AA)/GO hydrogel composite.

occurred is related to weight loss (42.46% and 38.39%) at 350 °C and is thought to be attributable to the removal of certain low molecular weights molecules. The third stage of degradation began at about 530 °C and is responsible for the disintegration of the crosslinking structure. Thus, thermogravimetric analysis tests showed that the synthesized crosslinking has stronger thermal stability and a higher decomposition temperature than the pure GG and GNAGO-0 hydrogel. This improved heat stability of the grafted hydrogel networks might be attributed to the development of cross-links between various polymeric chains *via* covalent bonding of GO (GNAGO-3).[37]

3.3. Zero shear viscosity investigations

In order to understand the steady shear flow behaviour of the hydrogel, the steady-state viscosity with increasing shear rate is depicted in Fig. 3(a) for the pure GNAGO-0 and its nanocomposites with GO(GO) on varying the filler amounts. At ambient temperature, the steadiness changes with the shear rate for varied GO (GO) concentrations (ranging from 0 to 5 mg).

A shear-thinning behavior was observed for all samples and the effect of GO concentration on viscosity is significant. The viscosity increases with increasing GO concentration and decreases with shear rate. This is the most common behavior of a non-Newtonian fluid.

As seen in Fig. 3a, introducing GO (1 mg) at a low shear rate increased the viscosity, indicating the formation of physical contacts between GO and the hydrogel matrix that restricted hydrogel chain movement, resulting in a quick increase in viscosity. In other words, the considerable surface area of GO can operate as a multifunctional cross-linker, interacting with matrix hydrogel chains along AA and NIPA with MBA, causing the hydrogel network to cross-link further.[38] Viscosity will in general increase with GO concentration, inferable from the expanded entangling of disordered hydrogel chains at increasing concentrations. This approach could be perceived by the presence of innumerable hydroxyl and carboxyl group constructions in the GO, which can enhance mechanical strength for structure linking between polymer groups and GO,[39] as well as the presence of a carboxylic acid collecting in acrylic acid, which works with the development of a gel structure. The presence of GO in hydrogels can extremely help their toughness.[40] The observed viscosities of the GO suspensions are clearly decreased as the shear rate increases, as seen in Fig. 3a. This further shows that the highly concentrated GO suspensions show significant shear-thinning behaviour as a non-Newtonian fluid. As a result, a slight increase of viscosity was also observed with increasing GO concentration from 1 mg to 3 mg. Beyond this concentration (3 mg) the entanglement of the hydrogel matrix was found to decrease slightly indicating this concentration to be the maximum concentration. That is, at a GO concentration of 4 mg and 5 mg, the viscosity slightly decreases.[41]

Fig. S1 (ESI†) shows the effect of GO concentration on the thickness (viscosity) of hydrogels at room temperature for four different shear rates. At low shear rates (0.1 s^{-1}), the GO immediately increased the thickness, which was apparent at 1 mg concentration. The uniformity is extended as the GO

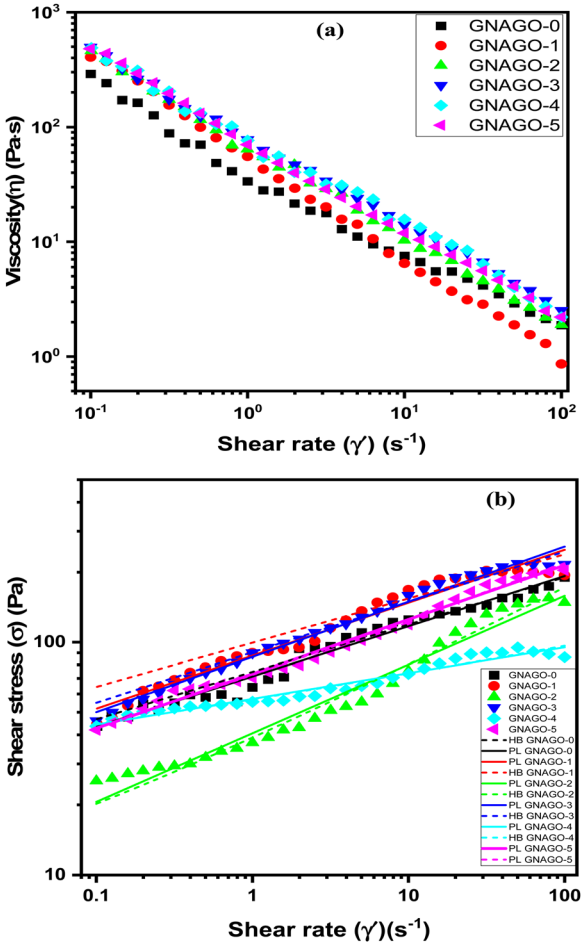

Fig. 3 Rheological profiles for (a) variation of viscosity with shear rate, and (b) superposition of rheological data and model curves obtained from the HB and PL model for GNAGO samples with different concentrations (0 to 5 mg).

concentration was increased up to 3 mg and after this concentration, the thickness somewhat decreases for 4 mg and 5 mg GO concentration because of the accomplishment of the soaking level of GO concentration. At a shear rate of 1 s^{-1}, thickness rises to somewhat less and reaches a proper arrangement of the hydrogel. At a high shear rate (100 s^{-1}), the thickness was less ineffective to increase in GO concentration. Table S1 (ESI†) depicts the data for the effect of GO concentration on the thickness of GNAGO hydrogels.

Fig. 3b presents the consistent shear stream bends of GO suspensions at different complexes. For shear rates more noteworthy than 0.1 s^{-1}, the GO suspensions behave as a non-Newtonian fluid, with shear stress increasing with shear rate. The steady flow behaviour was assessed by exposing the hydrogel to shear applied at different rates ranging from 0.01 to 100 s^{-1} and evaluating the effect and viscosity and shear stress of the hydrogel. The acquired data was used to obtain the values of parameters by using the following power law (eqn (1)) and the Herschel–Bulkley (eqn (2)) model equation:[42]

$$\tau = K\gamma^n \quad (1)$$

$$\tau = \tau_0 + K\gamma^n \quad (2)$$

where τ denotes shear stress (Pa), τ_0 designates the yield stress (Pa), K is the consistency coefficient (Pa s), γ is the shear rate (s^{-1}), and 'n' denotes the flow behaviour index (dimensionless). The results acquired from the data fitting are encapsulated in Table 1.

The yield stress values increase with GO concentration up to the GNAGO-3 hydrogel (1 mg to 3 mg) samples as after this for the GNAGO-4 and GNAGO-5 hydrogel samples the yield stress value decreases implying the maximum (peak) concentration of GO. In contrast, with an increase in the GO concentration, the viscosity decreases. This effect could be due to the formation of agglomerates of GO, which remarkably decreases the interaction between GO and the hydrogel, because of a decrease in the cross-linking in the network. The flow index, on the other hand, is usually less than one, indicating that shear-thinning behaviour is prominent in the suspensions. The rheological parameters derived using the PL and HB models for the GNAGO hydrogel samples at complete shear rate ranging from 0.1 to 100 s^{-1} are shown in Table S1 (ESI†).

The flow behaviour helps in understanding the effect of shear rate on power law parameters like, consistency coefficient (k) and flow behaviour index (n). It is apparent from the obtained rheological data that the shear stress of the GNAGO hydrogels increases with an increase in shear rate (Fig. 3b). Two mathematical models, *viz.* the power law and Herschel–Bulkley model, were fit to the obtained data to attain the value for 'k' and 'n'. The values for GNAGO hydrogels for different amounts of GO obtained from eqn (1) and (2) with a coefficient (R^2) are summarized in Table 1. It has been stated that 'k' is used for determining the water retention efficiency and viscosity of the hydrogel. In accordance with this fact, values of k were found to be in agreement with water binding. It can be inferred from the obtained data that all the hydrogels have $n < 1$. It is evident from the data that hydrogels in the current study have desirable flow behaviour indices. The similar values of k and n were obtained when the data was fitted in the Power law model and Herschel–Bulkley model. Since, the values of R^2 for all the samples (Table 1) are close to unity and both the Power law model and Herschel–Bulkley model show almost similar values obtained by fitting, we therefore assume that both models would be appropriate for consideration.[42]

3.4. Frequency sweep investigations

3.4.1. Complex viscosity study. Rheological characterizations are very important in presenting useful information about the dispersion state of particles, the interactions between particles, the polymer matrix, and also the partition threshold in a network structure. The rheological behavior is very much reactive to the variation in the structure of filled hydrogels in the low-frequency range. The penetration of GO can be detected by a sudden increase in the complex viscosity, which is associated with the formation of a filler network and pseudo-solid-like properties.[43,44]

Using 25 mm parallel plate geometry, a frequency sweep was undertaken at room temperature in the linear viscoelastic regime. Fig. 4 illustrates the complex viscosities of GNAGO hydrogels as a function of angular frequency. In the studied frequency range, the complex viscosity of neat GNAGO and GNAGO loaded with different concentrations of GO (1 mg to 5 mg) hydrogels exhibits non-Newtonian behaviour, indicating shear thinning in GNAGO and GNAGO loaded with GO (1 mg to 5 mg) hydrogels.[43] The complex viscosity followed a similar pattern to the shear viscosity and was highly dependent on the addition of GO. The linked network of GO and entangled molecular chains in the composites can be attributed to the shear thinning or pseudo-plastic behaviour observed in GNAGO with loaded GO hydrogels.[44] It is seen that as the GO is loaded into the hydrogel, the complex viscosity increases until the GO concentration of 3 mg irrespective of the frequency. Furthermore, an increase in the GO concentration (*e.g.* 4 mg and 5 mg) does not show an increase in the complex viscosity. These results may be attributed to the agglomeration of GO nanoparticles at higher concentrations. Table S2 (ESI†) displays the increased value of complex viscosity with added GO.

3.4.2. Storage and loss factor study. The frequency sweep is a well-known rheology measurement and is considered critical to the full characterization of fluid and soft hydrogels. These tests offer a basic understanding of the physical strength and cohesiveness of the fluid and gels. The tests typically determine storage modulus, and loss modulus as a function of frequency expressed in radians or hertz.[45]

Table 1 The rheological parameters obtained for Power law and Herschel–Bulkley at different concentrations of GNAGO hydrogels at room temperature with the calculated coefficient of determination (R^2)

	Power law			Herschel–Bulkley		
Sample code	k	n	R^2	k	n	R^2
GNAGO-0	71.26397	0.21575	0.97297	74.57298	0.20323	0.9756
GNAGO-1	87.5407	0.22749	0.96003	99.52267	0.18989	0.91347
GNAGO-2	40.62656	0.29514	0.96481	34.24965	0.34434	0.96762
GNAGO-3	86.49082	0.23706	0.98661	90.49638	0.21642	0.97019
GNAGO-4	57.11629	0.11052	0.95404	44.9608	0.13729	0.94274
GNAGO-5	73.11896	0.23339	0.98984	67.1577	0.2509	0.98826

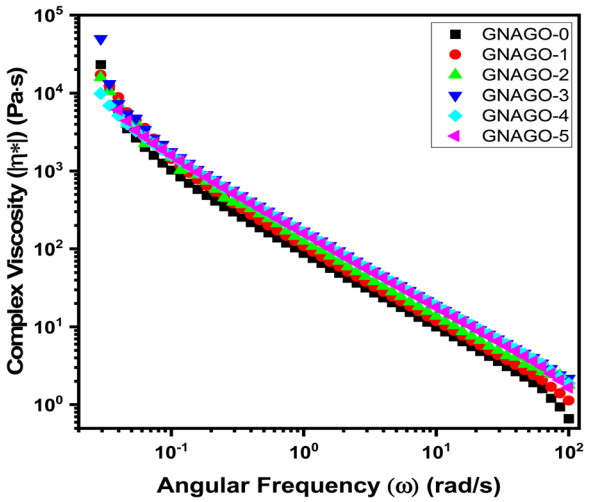

Fig. 4 Complex viscosity ($|\eta^*|$) *versus* angular frequency (ω) for (■) GNAGO-0, (●) GNAGO-1, (▲) GNAGO-2, (▼) GNAGO-3, (◆) GNAGO-4 and (◀) GNAGO-5 hydrogels.

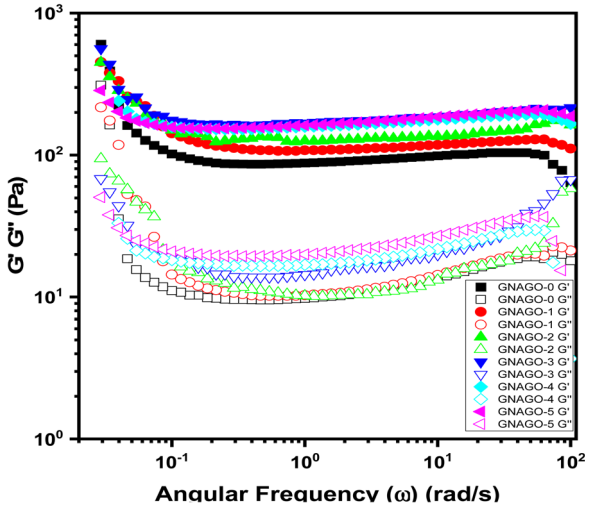

Fig. 5 Storage modulus (closed) (G') and loss modulus (open) (G'') *versus* angular frequency for (■) (□) GNAGO-0, (●) (○) GNAGO-1, (▲) (△) GNAGO-2, (▼) (▽) GNAGO-3, (◆) (◇) GNAGO-4 and (◀) (◁) GNAGO-5 hydrogels.

The angular frequency dependence of the storage modulus (G') and loss modulus (G'') for GNAGO hydrogels at 0 to 5 mg of GO is depicted in Fig. 5. All the GNAGO hydrogel samples showed that G' is greater than G'' and both moduli are practically independent of frequency, which is a mechanical spectrum characteristic of gels.[46] The clear huge difference between G' and G'', as well as the minor rise in G' with frequency, reveals the dynamic and elastic natures of the GNAGO hydrogel's self-cross-linking. The frequency sweep measurement was performed at room temperature and 10% strain while varying the frequency (Fig. 5). The results indicated that as the level of GO solution in the mixture was higher, the G' and G'' of GNAGO hydrogels rose. However, as the frequency was raised, there was a quick increase in G' and G''. The ensuing increase in moduli as GO loadings increase is due to the confinement effect and interaction between the hydrogel and GO. The change in moduli is significant at low frequencies, which narrows further with increasing frequency, and a sudden change in the storage modulus was observed between 0 and 3 mg, indicating that nanocomposites have reached a rheological percolation threshold at which GO hinders the motion of the polymer chain.[43]

3.5. Damping factor measurements

Fig. 6 shows the damping factor (loss tangent or tan δ) as a function of angular frequency at room temperature determined using eqn (3), which is really the ratio of G'' to G'.[47]

$$\tan\delta = G''/G' \quad (3)$$

Based on internal friction, this ratio offers information on the viscous and elastic characteristics of the material. The tan $\delta > 1$ value indicates that G'' has a higher value than G' and that the material is more viscous, allowing for more energy dissipation; however, the tan $\delta < 1$ value indicates that G' has a greater value than G'' and that the material is elastic. The tan $\delta = 1$ value indicates that the internal friction is independent of the applied strain and provides the gel point value. The calculated values of tan δ for GNAGO hydrogel samples are depicted in Table S2 (ESI†). The tan δ values for all the GNAGO hydrogels were slightly decreased up to a frequency of 10 rad sec^{-1}. Beyond this frequency, the tan δ values seem to be increased with the increase in the frequency, which indicates the stability and mechanical strength of the dispersed GO particles. The tan δ values for GNAGO-0, GNAGO-1, GNAGO-2, and GNAGO-3 hydrogel samples were found to be increased with the increase in the frequency due to the interlocking and penetration of GO particles in the hydrogels, while for GNAGO-4, and GNAGO-5 hydrogels the tan δ values decrease with the increase in the frequency which may be due to the decrease in the thickness of the hydrogel. The tan δ values as per Table S2 (ESI†) indicate that the hydrogel samples are elastic in nature. Furthermore, as the frequency increases, the loss tangent (eqn (3)) falls, supporting the creation of a rigid structure. This can occur when the density of the cross-linking varies, causing the rheological characteristics to shift.[48]

3.6. Rheological behaviour in the temperature sweep study

Temperature-dependent measurements of G' and G'' show not only the gel strength but also the gelation temperature. The temperature sweep experiment was carried out to evaluate the temperature sensitivity of GNAGO hydrogels in the temperature range of 15–60 °C at a frequency of 10 rad sec^{-1} and a heating rate of 2 °C per minute.[49] Fig. 7 indicates that when the GO concentration increases, so does the complex viscosity. The complex viscosity of a pure GNAGO hydrogel sample is maintained parallel to temperature up to 35 °C, while a significant spike is noticed above this temperature. For the GNAGO-1 hydrogel sample, the complex viscosity remained unchanged up to a temperature of 30 °C, and beyond this temperature, a slight increase in the complex viscosity was observed, which may be attributed to the lower concentration of GO. The complex viscosity

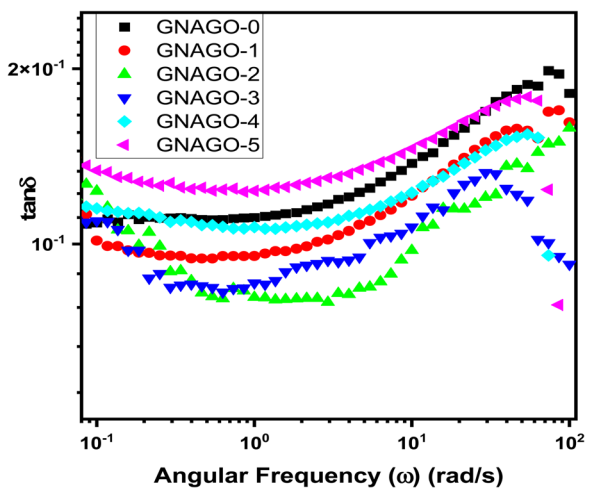

Fig. 6 Damping factor against angular frequency for (■) GNAGO-0, (●) GNAGO-1, (▲) GNAGO-2, (▼) GNAGO-3, (◆) GNAGO-4 and (◀) GNAGO-5 hydrogels.

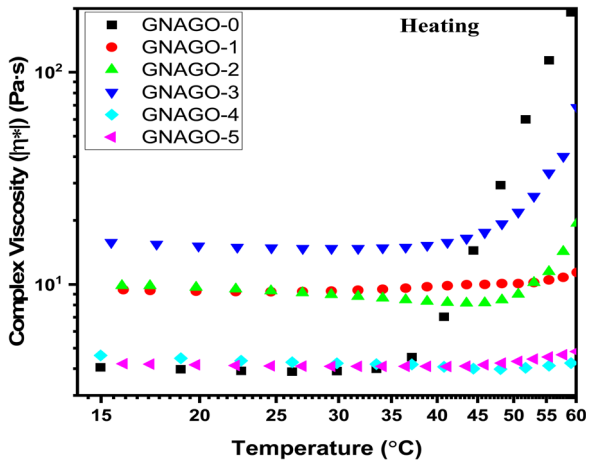

Fig. 7 Complex viscosity against temperature (heating) profile for (■) GNAGO-0, (●) GNAGO-1, (▲) GNAGO-2, (▼) GNAGO-3, (◆) GNAGO-4 and (◀) GNAGO-5 hydrogels.

of the GNAGO-2 and GNAGO-3 hydrogels increased at temperatures of 50 °C and 45 °C, respectively. The complex viscosity of the remaining hydrogel samples (GNAGO-1, GNAGO-4, and GNAGO-5) does not rise across the prescribed temperature range.

Fig. 8 represents the storage modulus (G') and loss modulus (G'') as a function of temperature for pure GNAGO hydrogel and GNAGO hydrogels with different concentrations of GO (1–5 mg). The storage modulus is obviously higher than the loss modulus as observed from the plot. The figure revealed that the hydrogels were intact in the temperature range of 10–35 °C. Beyond this, the temperature storage and loss modulus start increasing. At this temperature, the gel remained parallel to the temperature with significant gelation.[50] That is, the hydrogels retained their physical nature.[51] The coalescing of the hydrogel starts above 45 °C. The G' readings began to plateau at about 45 °C, indicating self-association of the GO

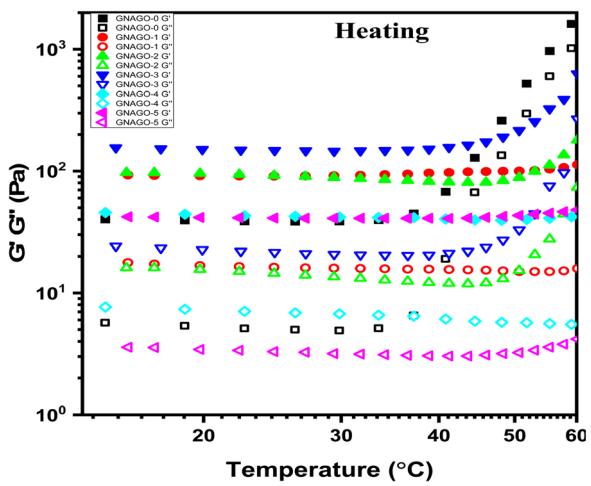

Fig. 8 Temperature sweep profiles of storage modulus (closed) and loss modulus (open) for (■) (□) GNAGO-0, (●) (○) GNAGO-1, (▲) (△) GNAGO-2, (▼) (▽) GNAGO-3, (◆) (◇) GNAGO-4 and (◀) (◁) GNAGO-5 hydrogels.

hydrogel. This is due to the fact that at higher temperatures, the hydrogen bond strength between GO and gum ghatti weakens, resulting in self-association.[51] From Fig. 8, the hydrogel sample GNAGO-3 acquires the maximum storage and loss modulus values. The data showing the storage and loss modulus for GNAGO hydrogel temperatures of 40 °C and 60 °C for the heating region is depicted in Table S3 (ESI†).

3.7. Linear viscoelastic investigations (LVR)

To assess the linear viscoelastic region (LVR), a strain sweep test (Fig. 9a) was carried out at a frequency of 10 rad s^{-1}, from which a suitable strain was chosen for confirming the oscillatory experiments. The hydrogel viscoelastic characteristics were examined by observing the progress of the influential moduli, G' and G''. The storage modulus (G') growth gives data about the sample solid-like behaviour, though the loss modulus (G'') increase gives data about the sample's liquid-like-behaviour. As far as possible for experiments acquired from ability, clear evidence is somewhere in the range of 1 and 10%. Fig. 9a similarly shows that the increase of GO in the GNAGO hydrogels did not change the common viscoelastic behavior of the

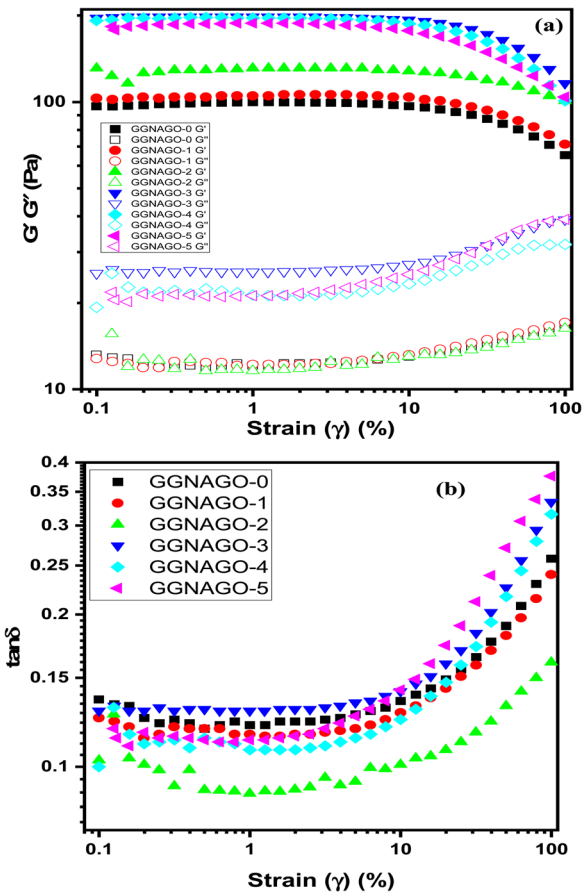

Fig. 9 (a) Storage modulus (closed) and loss modulus (open) as a function of strain for (■) (□) GNAGO-0, (●) (○) GNAGO-1, (▲) (△) GNAGO-2, (▼) (▽) GNAGO-3, (◆) (◇) GNAGO-4 and (◀) (◁) GNAGO-5 and (b) tan δ as a function of strain for (■) GNAGO-0, (●) GNAGO-1, (▲) GNAGO-2, (▼) GNAGO-3, (◆) GNAGO-4 and (◀) GNAGO-5 hydrogels.

hydrogels, however, absolutely affected the G' as well as G'' at low strain range for GO up to 3 mg. However, the GNAGO-4 and GNAGO-5 hydrogels showed low values of G' and G'' as compared to the GNAGO-3 hydrogel. The rheological data discussed above confirmed that GO strengthened the effect of internetwork interactions.[52]

Fig. 9b represents the variation of tan δ against the change of strain amplitude. The tan δ value of the GNAGO hydrogel increases with the increase of strain % as the value of G″ increased with strain %. The change of tan δ values is in the range of 0.1–10% strain. As seen in Fig. 9b the tan δ values for all the GNAGO hydrogels remained unchanged (remained parallel to strain %) up to 10% strain. But, as the strain is increased from 10% to 100% the tan δ values showed a sudden rise. The GNAGO (0–5) G' values were more than the loss moduli G'', however the loss factor and tan δ values were less than 1. This result shows that all GNAGO (0–5) samples exhibited a more elastic structure rather than a viscous character over a broad range of strain, and the values for the same are shown in Table S4 (ESI†). tan δ (G''/G'), the phase angle, indicates the viscoelastic configuration of the samples and denotes two different circumstances for a material: tan $\delta > 1$ indicates that the material has a viscous behavior and tan $\delta < 1$ shows the elasticity behavior of the system.[53,54]

3.8. Shear stress–strain (%) study

Fig. 10 represents the shear stress *versus* strain measurements for GNAGO (0 to 5) hydrogels. It is seen that the shear stress constantly increases with the increase in strain. For the pure GNAGO-0 sample, the observed stress value at the very least strain (for 0.1% strain) is 0.0971 pa. As the strain is increased from 1%, to 10%, 25.1%, and 99.8%, the stress constantly continues to increase (1 pa, 9.76 pa, 22.9 pa, and 67.2 pa). As the concentration of GO is increased from 1 mg to 5 mg, the GNAGO-3 hydrogel sample showed the most extreme stress value of 0.198 pa, 1.99 pa, 19.4 pa, 45.4 pa, and 122 pa at a strain of 0.1, 1.0, 10, 25.1 and 99.8% (Table S5, ESI†). This large value of the hydrogel (GNAGO-3) demonstrates that the GO is very much dispersed in the gel, which shows better crosslinking giving the most cohesion to the hydrogel study.[55] On further addition of GO (4 mg to 5 mg) for the said strain values, there was a slight change in the stress as the hydrogels (GNAGO-4 and GNAGO-5) observed a steady value of strain when compared with pure hydrogel indicating the higher mechanical strength stability of the hydrogels.

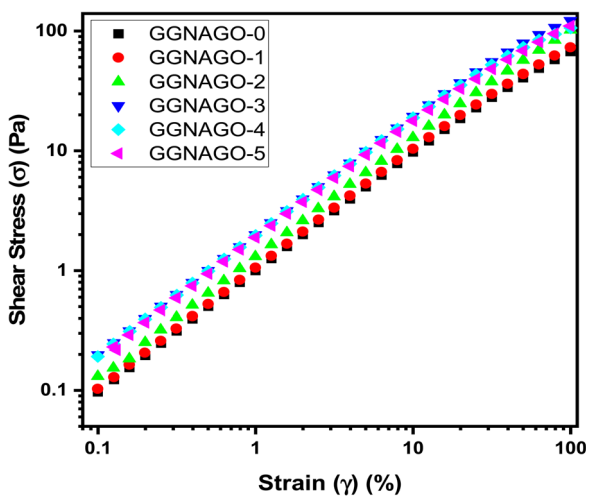

Fig. 10 Shear stress (σ) *vs.* strain (%) for (■) GNAGO-0, (●) GNAGO-1, (▲) GNAGO-2, (▼) GNAGO-3, (◆) GNAGO-4 and (◀) GNAGO-5 hydrogels.

4. Conclusions

Utilizing SEM and TGA methods, a gum ghatti-cl-poly(*N*-isopropylacrylamide-*co*-acrylic acid)/GO hydrogel was successfully characterised. The synthesized hydrogel mixture's rheological characteristics were thoroughly studied. Shear thinning behaviour may be shown in the flow curve (shear rate, viscosity, and shear stress) and flow sweep study of the GG-cl-poly(NIPA-*co*-AA)/GO hydrogel. The GG-cl-poly(NIPA-*co*-AA)/GO exhibits elastic behaviour and has gel-like properties, as shown by the storage modulus (G') and loss modulus (G'') values of the studies. It was seen that adding GO particles to the hydrogel network enhanced the materials mechanical characteristics and made them the strongest surface adsorption active components. The velocity profiles of the gel were investigated using rheological models, although the Herschel–Bulkley and Power laws were the best fit for the data. The rheological analysis suggested that these materials may be utilized in the field for controlled drug loading and release because of the presence of GO. The GG-cl-poly(NIPA-*co*-AA)/GO is cationic because it includes an anionic polymer and GO. These characteristics reduce the hydrophilic property of the materials and neutralise the charge components, making them appropriate for anionic drug loading. In addition to its ability to carry drugs, the hydrogel rheology implies that it could be a superior carrier for drug delivery.

Conflicts of interest

There are no conflicts to declare.

Acknowledgements

The authors are thankful for the Shodh fellowship provided by the government of Gujarat and to the Department of Chemistry for the laboratory and instrumental facilities. The authors are also thankful to the Department of Physics and CISST Department, Sardar Patel University, V. V. Nagar, for various analyses.

References

1 Y. Zhu, S. Murali, W. Cai, X. Li, J. W. Suk, J. R. Potts and R. S. Ruoff, *Adv. Mater.*, 2010, **22**, 3906–3924.
2 A. Amir, S. Mahalingam, X. Wu, H. Porwal, P. Colombo, M. J. Reece and M. Edirisinghe, *Compos. Sci. Technol.*, 2016, **129**, 173–182.

3 Y. Piao and B. Chen, *Int. J. Biol. Macromol.*, 2017, **101**, 791–798.
4 L. A. Shah, T. U. Rehman and M. Khan, *Polym. Bull.*, 2020, **77**, 3921–3935.
5 J. H. Lee, J. Ahn, M. Masuda, J. Jaworski and J. H. Jung, *Langmuir*, 2013, **29**, 13535–13541.
6 H. Mittal and S. B. Mishra, *Carbohydr. Polym.*, 2014, **101**, 1255–1264.
7 A. S. Deshmukh, C. M. Setty, A. M. Badiger and K. S. Muralikrishna, *Carbohydr. Polym.*, 2012, **87**, 980–986.
8 G. C. M. A. Diego Aires da Silva and R. da S. Pena, *Innovation in the Food Sector Through the Valorization of Food and Agro-Food By-Products*, 2020, 32, 1–24.
9 L. A. Shah, K. Gul, I. Ali, A. Khan, S. Muhammad, M. Ullah, I. Bibi and S. Sultana, *Iran. Polym. J.*, 2022, **31**, 845–856.
10 I. Ali and L. A. Shah, *Polym. Bull.*, 2021, **78**, 1275–1291.
11 L. Li, P. S. Liu, N. L. Zhou, J. Zhang, S. H. Wei and J. Shen, *J. Appl. Polym. Sci.*, 2006, **102**, 5725–5730.
12 C. Li, M. She, X. She, J. Dai and L. Kong, *J. Appl. Polym. Sci.*, 2014, **131**, DOI: **10.1002/app.39872**.
13 G. R. Bardajee, F. Mizani and S. S. Hosseini, *J. Polym. Res.*, 2017, **24**, DOI: **10.1007/s10965-017-1197-4**.
14 G. R. Bardajee, S. S. Hosseini and S. Ghavami, *J. Inorg. Organomet. Polym. Mater.*, 2018, **28**, 2196–2205.
15 G. Rezanejade Bardajee, S. Sadat Hosseini and C. Vancaeyzeele, *New J. Chem.*, 2019, **43**, 3572–3582.
16 M. Fang, K. Wang, H. Lu, Y. Yang and S. Nutt, *J. Mater. Chem.*, 2009, **19**, 7098–7105.
17 M. Castelaín, G. Martínez, C. Marco, G. Ellis and H. J. Salavagione, *Macromolecules*, 2013, **46**, 8980–8987.
18 A. A. Vasileiou, M. Kontopoulou and A. Docoslis, *ACS Appl. Mater. Interfaces*, 2014, **6**, 1916–1925.
19 L. A. Shah, T. U. Rehman and M. Khan, *Polym. Bull.*, 2020, **77**, 3921–3935.
20 B. Yu, X. Wang, X. Qian, W. Xing, H. Yang, L. Ma, Y. Lin, S. Jiang, L. Song, Y. Hu and S. Lo, *RSC Adv.*, 2014, **4**, 31782–31794.
21 H. M. Seo, J. H. Park, T. D. Dao and H. M. Jeong, *J. Nanomater.*, 2013, **2013**, 9–11.
22 V. Mittal and A. U. Chaudhry, *Colloid Polym. Sci.*, 2016, **294**, 1659–1670.
23 C. A. Tao, J. Wang, S. Qin, Y. Lv, Y. Long, H. Zhu and Z. Jiang, *J. Mater. Chem.*, 2012, **22**, 24856–24861.
24 K. M. Park, J. A. Yang, H. Jung, J. Yeom, J. S. Park, K. H. Park, A. S. Hoffman, S. K. Hahn and K. Kim, *ACS Nano*, 2012, **6**, 2960–2968.
25 H. Gao, Y. Sun, J. Zhou, R. Xu and H. Duan, *ACS Appl. Mater. Interfaces*, 2013, **5**, 425–432.
26 Y. Sun, Q. Wu and G. Shi, *Phys. Chem. Chem. Phys.*, 2011, **13**, 17249–17254.
27 C. Huang, H. Bai, C. Li and G. Shi, *Chem. Commun.*, 2011, **47**, 4962–4964.
28 L. A. Shah, T. U. Rehman and M. Khan, *Polym. Bull.*, 2020, **77**, 3921–3935.
29 E. Makhado, S. Pandey and J. Ramontja, *Int. J. Biol. Macromol.*, 2018, **119**, 255–269.
30 B. Kamaliya, P. N. Dave and P. M. Macwan, *Polym. Bull.*, 2023, **80**, 6923–6944.
31 B. Sharma, S. Thakur, D. Trache, H. Y. Nezhad and V. K. Thakur, *Nanomaterials*, 2020, **10**, 1–22.
32 S. Gopi, A. Rajeswari, G. Sudharsan and A. Pius, *J. Water Process Eng.*, 2019, **31**, 100850.
33 B. Li, T. Liu, L. Hu, Y. Wang and S. Nie, *Chem. Eng. J.*, 2013, **215–216**, 819–826.
34 E. Makhado, S. Pandey and J. Ramontja, *Int. J. Biol. Macromol.*, 2018, **119**, 255–269.
35 K. Sharma, V. Kumar, B. Chaudhary, B. S. Kaith, S. Kalia and H. C. Swart, *Polym. Degrad. Stab.*, 2016, **124**, 101–111.
36 K. Sharma, B. S. Kaith, V. Kumar, S. Kalia, V. Kumar, S. Som and H. C. Swart, *eXPRESS Polym. Lett.*, 2014, **8**, 267–281.
37 S. D. Sahoo and E. Prasad, *Soft Matter*, 2020, **16**, 2075–2085.
38 A. Narimani, F. Kordnejad, P. Kaur, S. Bazgir, M. Hemmati and A. Duong, *J. Polym. Eng.*, 2021, **41**, 788–798.
39 C. Pan, L. Liu, Q. Chen, Q. Zhang and G. Guo, *ACS Appl. Mater. Interfaces*, 2017, **9**, 38052–38061.
40 S. Rahmani, A. Olad and Z. Rahmani, *Polym. Bull.*, 2022, **80**, 4117–4138.
41 A. Narimani, F. Kordnejad, P. Kaur, S. Bazgir, M. Hemmati and A. Duong, *J. Polym. Eng.*, 2021, **41**, 788–798.
42 A. R. Choudhury, *Int. J. Biol. Macromol.*, 2020, **156**, 591–597.
43 S. N. Tripathi, R. S. Malik and V. Choudhary, *Polym. Adv. Technol.*, 2015, **26**, 1558–1566.
44 A. Kumar, K. M. Rao and S. S. Han, *Carbohydr. Polym.*, 2018, **193**, 228–238.
45 K. Alam, M. Iqbal, A. Hasan and N. Al-Maskari, *J. Appl. Biotechnol. Rep.*, 2020, **7**, 172–176.
46 B. T. Tomoda, M. S. Pacheco, Y. B. Abranches, J. Viganó, F. Perrechil and M. A. De Moraes, *Polymers (Basel)*, 2021, **13**, 798.
47 T. Ur Rehman and L. Ali Shah, *Z. Phys. Chem.*, 2021, **235**, 329–343.
48 S. Soltani, R. Emadi, S. H. Javanmard, M. Kharaziha, A. Rahmati, V. K. Thakur and S. Lotfian, *Gels*, 2022, **8**, 121.
49 W. Du, L. Tan, Y. Zhang, H. Yang and H. Chen, *Int J. Polym. Sci.*, 2019, 1–10.
50 Ö. Demir Oğuz and D. Ege, *J. Ankara Univ. Faculty of Medicine*, 2018, **71**, 172–176.
51 K. Phogat, S. Kanwar, D. Nayak, N. Mathur, S. B. Ghosh and S. Bandyopadhyay-Ghosh, *J. Appl. Polym. Sci.*, 2020, 137.
52 S. Tarashi, H. Nazockdast and G. Sodeifian, *Polymer*, 2019, 183.
53 B. Kamaliya, P. N. Dave and P. M. Macwan, *J. Appl. Polym. Sci.*, 2022, **139**, DOI: **10.1002/app.52888**.
54 M. Fathollahi and H. Bouhendi, *J. Polym. Res.*, 2023, **30**, 172.
55 S. Bashir, Y. Y. Teo, S. Ramesh and K. Ramesh, *Polymer*, 2018, **147**, 108–120.